ACS OMEGA

http://pubs.acs.org/journal/acsodf

Article

Study on the Mechanics and Pore Characteristics of Coal Seam Drilling Sealing Materials Based on Nanomaterial Optimization

Dahe Yu and Jun Xie*

Cite This: *ACS Omega* 2022, 7, 27991−28002

Read Online

ACCESS | Metrics & More | Article Recommendations

ABSTRACT: In order to modify and optimize the performance of cement-based sealing materials and improve the gas drainage rate of boreholes. In this paper, nanosilica (NS), multiwalled carbon nanotubes (MWCNT), and graphene oxide (GO) were used to modify cement and optimize the pore structure. Uniaxial compression tests, X-ray diffraction (XRD), nuclear magnetic resonance (NMR), and combined fractal theory were used to analyze the mechanics and pore characteristics. The results show that the synergy of the three nanomaterials promotes the generation of hydration products such as calcium silicate hydrate (C−S−H) and ettringite (AFt), improves the total pore fractal dimension (D_w) and seepage pore fractal dimension (D_s), and optimizes the microscopic pore structure. However, when the content of NS increases from 2 to 4 wt %, the improvement in the mechanical properties is obviously weakened. The best ratio is where the SiO_2 content is 2 wt %, the MWCNT content is 0.1 wt %, and the GO content is 0.03 wt %. Compared with pure cement, the fractal dimension increases significantly, the mechanical properties are increased by 24.7%, and the total porosity is reduced by 23.9%. This paper is of great significance for improving the efficiency of gas mining.

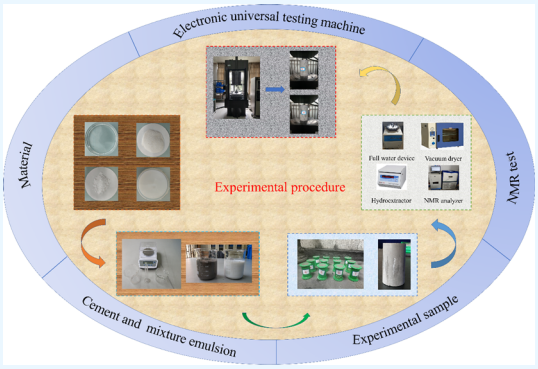

1. INTRODUCTION

To effectively curb the occurrence of coal mine gas accidents, China often adopts technical means of gas drainage to reduce the gas concentration in the mine. With the further development of research, the performance of sealing materials has gradually become the main factor affecting the sealing effect of drilling holes.[1,2] Cement material is widely used in construction, coal, oil, transportation, and other fields due to its advantages of low costs and easy availability. However, in the field of sealing materials, the inherent mechanical properties and pore structure of ordinary cement material cannot meet the production needs. In recent years, with the development of chemical material science and technology, the modification of cement mortar has received increasing attention from researchers and the preparation technology of ultrafine cement, special cement, and other materials has begun to develop vigorously.[3,4] Through research on the modification of cement mortar, materials such as high-expansion multiple cement mortar, high-strength cement mortar, and water-soluble polyurethane cement mortar have been developed. To a certain extent, mortar retains the advantages of compressive resistance, shear resistance, and high strength of cement-based materials and can compensate for the dry shrinkage, rich cracks, and poor sealing effect.[5,6] However, at this stage, the performance of the sealing material still fails to meet the production needs. Therefore, it is necessary to continue the research and development of cement-based sealing materials based on the original to optimize their performance.

To improve the performance of cement materials, predecessors have conducted a series of studies. Li et al. found that a certain amount of nanosilica (NS) can promote the early hydration process of cement and form a dense microstructure.[7] Zhang et al. found that NSs not only consume a large amount of calcium hydroxide (CH) to form a dense calcium silicate hydrate (C−S−H) gel but also play a role in graded filling to improve the microstructure and mechanical properties.[8] Kooshafar et al. found that nanosilica sol has a strong condensation in the pore space environment and the addition of nanosilica gel and fine aggregates has a higher role in promoting cement hydration.[9] Fernández and authors believed that the addition of NS promoted the formation of C−S−H gel by a pozzolanic reaction with CH.[10] The formation of the C−S−H gel and the filling effect of NS enhanced the densification of the binding matrix. Arrechea et al. found that by adding 0.01 wt % MWCNTs, the peak stress of the modified material at 7 and

Received: March 29, 2022
Accepted: July 6, 2022
Published: August 5, 2022

28 days was increased to 26.7 and 35.9 MPa and, compared with pure cement specimens, the peak stress increased by 5.26% and 2.02%, respectively.[11] Jeevanagoudar et al. found that the maximum Young's modulus of MWCNTs can reach 1 TPa, which have great stiffness, strength, and aspect ratios and are a good reinforcing material in mechanical properties.[12] According to research by Shi et al.,[13] MWCNTs are a nanostructured fiber material with excellent properties and their dispersion degree is a decisive factor affecting the properties of composite materials. Long et al. found that GO can promote hydration of cement, refine the pore structure, reduce the pore content and improve the density of cement slurry.[14] Chen et al. showed that GO, which contains rich carboxyl, hydroxyl, and epoxy functional groups, can interact with hydration products, forming a strong covalent bond at the cement interface thereby improving the mechanical properties of the material.[15]

In recent years, a series of studies has shown that the addition of nanofillers promotes the formation of hydration products, improves the compactness of sealing materials, optimizes the pore structure, reduces the formation of primary cracks and pores, and improves the compressive strength of composites.[16−19] Therefore, nanomaterials show good potential in improving the microstructure characteristics and mechanical properties of cement composite materials. To date, research on the strengthening of cement-based materials has emerged, but there are few reports on related articles about optimizing the pore structure and improving the performance of sealing materials through the synergistic effect of a variety of nanomaterials.[20−23]

Therefore, the purpose of this paper is to study the mechanical properties, strengthening mechanism, and microstructure of cement sealing materials modified by MWCNTs, GO, and SiO_2 nanomaterials. Using uniaxial compression, XRD, NMR, and fractal theory, the mechanical properties, reinforcement mechanism, and microstructure of the modified materials were qualitatively and quantitatively analyzed. This paper is of great significance to the development of borehole sealing materials and the improvement of gas drainage efficiency.

2. EXPERIMENTAL STUDIES

2.1. Material Selection and Experimental Method. The main raw materials of sealing materials are cement, ordinary tap water, nanosilica (NS), multiwalled carbon nanotubes (MWCNTs), and graphene oxide (GO). NS is a nontoxic, tasteless, nonpolluting new inorganic chemical material that can improve the aging resistance and chemical resistance of other materials.[24−26] The addition of NS into cement can promote the formation of calcium silicate hydrate and improve the strength of the material. Because the carbon atoms in MWCNTs adopt sp^2 hybridization and have the characteristics of a high modulus and high strength, multiwalled carbon nanotubes have good tensile and compressive properties.[27−29] GO has the advantages of a large specific surface area, excellent surface chemical properties, and hydrophilicity and can improve the strength and toughness of composites by synergistic action with other materials.[30−32] In this experiment, MWCNTs with a particle size of 10,000 mesh NS, a sheet diameter of <30 μm, a sheet thickness of 1 nm, an outer diameter of 8−15 nm, an inner diameter of 3−5 nm, and a length of 3−12 μm were selected as the sealing modification material. In addition, the bulk density of MWCNTs is 0.15 g/cm^3, and the actual density is 2.1 g/cm^3. MWCNTs are difficult to dissolve in water. Therefore, PVP is added as a dispersant to make it soluble in water, and ultrasonic dispersion technology is used to improve the dispersion uniformity of the solution.

According to the relevant requirements of sealing, strength, and fluidity of drilling sealing materials combined with the advantages of a variety of nanomaterials and cement, the optimal mix of materials was screened by orthogonal testing, as shown in Table 1. The water−cement ratio selected in the experiment was 0.5, and the experimental equipment and process are shown in Figure 1.

Table 1. Material Composition of Each Experimental Group

	category		
serial no.	SiO_2 (wt %)	MWCNTs (wt %)	GO (wt %)
#0	0	0	0
#1	1	0.1	0.03
#2	2	0.05	0.03
#3	2	0.1	0.01
#4	2	0.1	0.03
#5	4	0.05	0.03

The mass ratio of polyvinylpyrrolidone (PVP) dispersant to MWCNTs was 6%. First, the PVP dispersant was weighed according to different MWCNT ratio schemes and added into water and quickly stirred to make it completely dissolved in water. Then, MWCNTs, GO, and NS were added into water in turn according to the proportion shown in Table 1 and quickly stirred for 5 min with a stirrer. The stirred solution was placed in an ultrasonic cleaner for 15 min to disperse and then poured into a beaker with cement and stirred well. The stirring solution was dispersed into an ultrasonic cleaner for 15 min and finally poured into a beaker and stirred with cement until the material was evenly mixed. The uniformly mixed slurry was poured into a 50 × 100 cylindrical mold and demolded after standing for 48 h. Then, the solutions were maintained for 28 days in a standard curing environment with a temperature of 20 ± 2 °C and relative humidity of ≥95%. After curing, the samples were placed in anhydrous ethanol to terminate hydration. Before the NMR relaxation test, the samples were vacuum-saturated with water for 12 h. When the sample was completely saturated by water, the T_2 spectrum in the saturated water state was measured, and then the saturated water samples were centrifuged and dried to detect the T_2 spectra in the residual state. After the nuclear magnetic resonance test was completed, the mechanical properties and hydrate content of the sample were tested.

2.2. Experimental Apparatus. Figure 2 shows different pore characterization methods with a wider range of NMR measurements and no negative impact on the pore and mechanical properties of the sample, so this paper uses NMR to characterize the pore structure. In this study, the low-field nuclear magnetic resonance analyzer used is the MesoMR low-field nuclear magnetic resonance analyzer produced by Suzhou Niumag Analytical Instrument Corporation by which the nuclear magnetic resonance test is carried out. The main magnetic field intensity is 0.5 ± 0.05 T, the main frequency is 21.3 MHz, the RF power is 300 W, and the uniformity of the magnet is 12.0 × 10^{-6}. The pore structure of the cement specimen was studied by the volume relaxation method (transverse relaxation time T_2).

For the uniaxial compression mechanics experiment, a Shimadzu AGX-250 electronic universal testing machine produced by Shimadzu Analytical Instrument Company is adopted. The loading mode of the device is divided into the

https://doi.org/10.1021/acsomega.2c01900
ACS Omega 2022, 7, 27991−28002

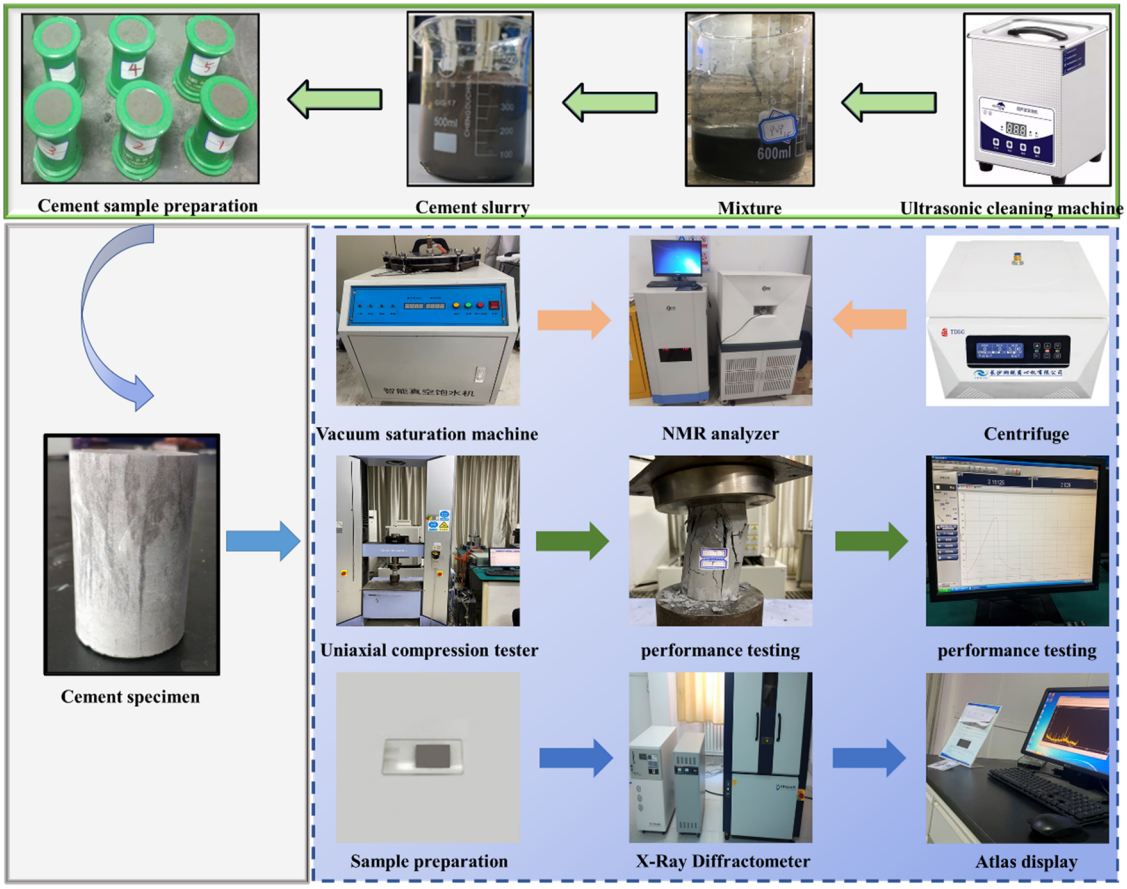

Figure 1. Experimental process.

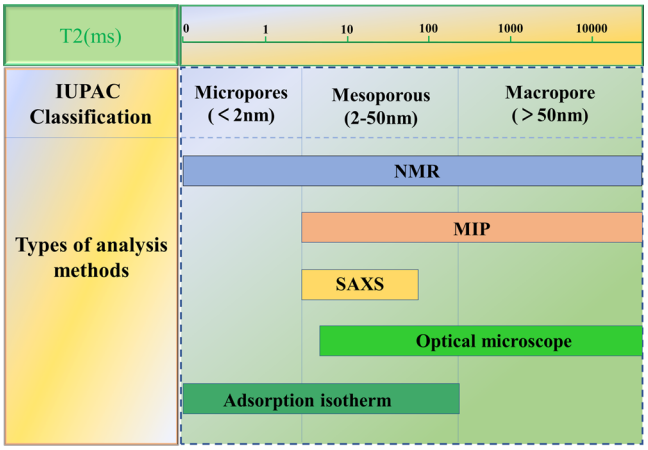

Figure 2. Different pore test methods and test scope.

displacement loading and stress loading, and the displacement loading is used in the experiment. The detailed experimental parameters of the equipment are as follows: loading speed of 0.05−100 mm/min, maximum sampling frequency of 3 s^{-1}, maximum load capacity of 120 KN, axial displacement of 100 mm, and load accuracy of ±0.3%.

The XRD experiment uses the D/Max2500PC X-ray diffractometer produced by Rigaku Corporation. Main technical parameters: angle range of 4−140°, angle reproducibility of ≤0.0001°. The maximum output power is 3 KW. In the scanning mode, the sample level does not move, and the minimum step of the THERA/THERA goniometer is 0.0001°.

In this experiment, a vacuum-drying furnace, vacuum water saturation device, centrifuge, high-precision electronic balance, and small mixer are also used.

2.3. Nuclear Magnetic Resonance Principle. NMR measurements are fast, noninvasive, and nondestructive and can be used to characterize cement specimens in imaging, relaxation, diffusion and other aspects. The transverse relaxation time (T_2) determined by the physical properties of materials and the characteristics of fluids is an important parameter in NMR experiments and is used to characterize the signal attenuation rate in pores.[33] Since the low-field NMR instrument is used in the experiment, the magnetic field gradient can be ignored. Thus, the transverse relaxation time T_2 can be expressed as

$$\frac{1}{T_2} \approx \frac{1}{T_{2s}} = \rho_2 \frac{S}{V} \quad (1)$$

In the formula, T_2 is the relaxation time of water in the pore; T_{2s} is the relaxation time of the surface; ρ_2 is the relaxation strength of the lateral surface of the rock; S is the total surface area of the rock pore; V is the pore volume; and S/V is the ratio of the pore surface area to volume.[34]

T_2 distribution is closely related to the pore size. The transverse relaxation time T_2 value is proportional to the pore radius, and the pore size distribution can be calculated from the distribution of the transverse relaxation time T_2 value.[35,36] The distribution of signal peaks in the T_2 spectrum reflects the development characteristics of material pores; the peak position reflects the pore size; the peak area reflects the pore volume; and the number of peaks reflects the continuity of pores at all levels.[37]

https://doi.org/10.1021/acsomega.2c01900
ACS Omega 2022, 7, 27991−28002

3. EXPERIMENTAL RESULTS AND DISCUSSION

3.1. Mechanical Property Analysis. A uniaxial compression test of the material was carried out to study the synergistic effect of the three nanomaterials screened by orthogonal experiments on the mechanical strength of the sealing material. Pure cement specimens and nanomaterial-modified cement specimens were selected for experiments and numbered #0, #1, #2, #3, #4, and #5. The sample number corresponds to the number in Table 1, and the original data for each specimen are shown in Table 2.

Table 2. Parameters of Experimental Samples

material number	sample length (mm)	sample diameter (mm)	sample quality (g)
#0	100.53	51.22	344.56
#1	101.11	50.46	382.43
#2	101.22	51.01	381.83
#3	100.19	50.95	382.05
#4	100.22	50.12	383.21
#5	100.08	50.33	381.65

Figure 3 shows the stress−strain curve obtained under the uniaxial compression test. The failure process of cement specimens under loading is divided into four stages. The OA section is the initial loading stage, the stress gradually increases from 0 MPa, and the specimen is gradually compacted until the cracks and pores are closed. The AB section is the stage when the specimen enters the stage of elastic deformation, and the stress−strain curve approximately changes to a straight line. The BC segment cracks entered the accelerated expansion stage. The internal portion and surface slightly crack and move as the stress increases, and the movement is intensified within a specific range until the peak stress is reached. Point C is the peak stress point, and after point C is the failure stage where the crack propagation is accelerated.

In the initial period of the OA segment, the original fractures and larger pores in the sample began to close under relatively small loads. With the continuous increase in stress, the cement specimens began to generate tiny cracks, and the slope of the curve began to increase to the end of point A.[38,39] Samples #1, #2, #3, #4, and #5 have different degrees of reduction in the initial loading stage compared with #0 of a pure cement specimen. The reduction in the initial loading stage indicates that the pores and cracks of the specimen are reduced, and the compactness and mechanical properties of the material are improved. Compounds #1 and #2 have a small decrease in the initial loading stage compared with the pure cement specimens; #3, #4, and #5 have a larger decrease, and #3 has the most obvious effect, indicating that the synergistic effect of adding three different ratios of nanomaterials to cement has a significant effect on reducing the cracks and macropores inside the cement parts. The reasons may be as follows: first, the addition of NS promoted the formation of hydrated calcium silicate, and MWCNTs bridged the hydration products and blocked the capillary pore structure, thus forming the overall network structure, improving the microstructure, and reducing the pore connectivity. Second, NS plays the role of ultrafine aggregate, filling the pores around the clinker and the pores of hydration products, thus optimizing the pore structure of the composites.[40,41] Furthermore, GO promotes the formation of tiny and regular hydrated crystal structures,[42] which reduces the number of large pores (>50 nm) and rapidly increases the number of smaller pores (<50 nm) so that the main pores of the cement slurry decrease and the pores tend to be uniform.[43]

After point A, the mixture began to enter the stage of elastic deformation, and with the continuous increase in load, the fracture and cracks in the cement sample began to spread uniformly. There is negligible impact on the integrity of the material within the limits it can withstand. The BC part is the accelerated crack propagation stage, the cracks continue to propagate in the vertical direction, and the cracks in the nonvertical direction begin to appear and cross with the cracks in the vertical direction. The integrity of the sample is compromised, and the fracture network displays unstable propagation in the sample until point C reaches the peak stress. After point C, the sample enters the destruction stage. The stored energy reaches the limit that the material can withstand and is quickly released outward, causing the fracture network connecting the longitudinal cracks and the transverse cracks to rupture, and the material loses its structural integrity.

Table 3 shows that the addition of various nanomaterials increases the early compressive strength. The mechanical properties of the cement specimens with curing periods of 7 and 28 days were relatively consistent, and the order of strength was #4 > # 2 > #3 > #1 > #5 > #0. The optimal proportioning scheme selected by orthogonal tests for the three different nanomaterials showed different degrees of improvement in the early and later mechanical properties compared with the pure cement specimens. Taking the curing period of 28 days as an example, the mechanical properties of #1, #2, #3, #4, and #5 increased by 8.93%, 21.05%, 16.31%, 24.7%, and 4.89%, respectively, compared with the mechanical properties of #0 of pure cement. The mechanical properties of the #4 modified material ratio scheme have the largest increase, while #5 has the smallest increase of 4.89%.

The comparison of different proportions of nanomodified materials found that, based on #1, #3 increased the SiO_2 ratio from 1 to 2 wt %, reduced the GO ratio from 0.03 to 0.01 wt %, and improved the mechanical properties by 7.38%. With #2 and #4 as the control group, we can conclude that the MWCNTs increased from 0.05 to 0.1 wt % and the compressive strength of the material increased by 3.65%. Comparing #4 and #3, the mechanical properties of GO content increased to 0.03 wt %, an increase by 8.39%. That is, the antipressure performance of 2 wt % SiO_2, 0.1 wt % MWCNTs, and 0.03 wt % GO within the range of the optimal ratio can be improved the most. Therefore, the optimal ratio of the synergistic effect of the three nanomaterials is 2 wt % SiO_2, 0.1 wt % MWCNTs, and 0.03 wt % GO as shown by the mechanical properties. The SiO_2 ratio of #5 increases from 2 to 4 wt %, the mechanical properties of #5 were slightly larger than those of pure cement specimens, and the improvement of mechanical properties was far less than that of other nanomodified materials. This is because the addition of SiO_2 in a certain range can consume a large amount of CH to form a dense C−S−H optimized pore structure, but excessive SiO_2 will cause agglomeration and reduce the uniformity of the specimen texture, which affects the peak stress.[44]

The modulus of elasticity can reflect the ability of the material to resist deformation. The greater the modulus of elasticity is, the stronger is the ability of the material to resist complex external factors.[45,46] The elastic moduli of experimental groups #1, #2, #3, #4, and #5 were 5.16, 5.30, 5.47, 5.65, and 5.02 GPa, respectively. Compared with the pure cement sealing material (4.97 GPa), the elastic modulus increased by 3.82%, 6.64%, 10.06%, 13.68%, and 1.01%. The relationship between the

https://doi.org/10.1021/acsomega.2c01900
ACS Omega 2022, 7, 27991−28002

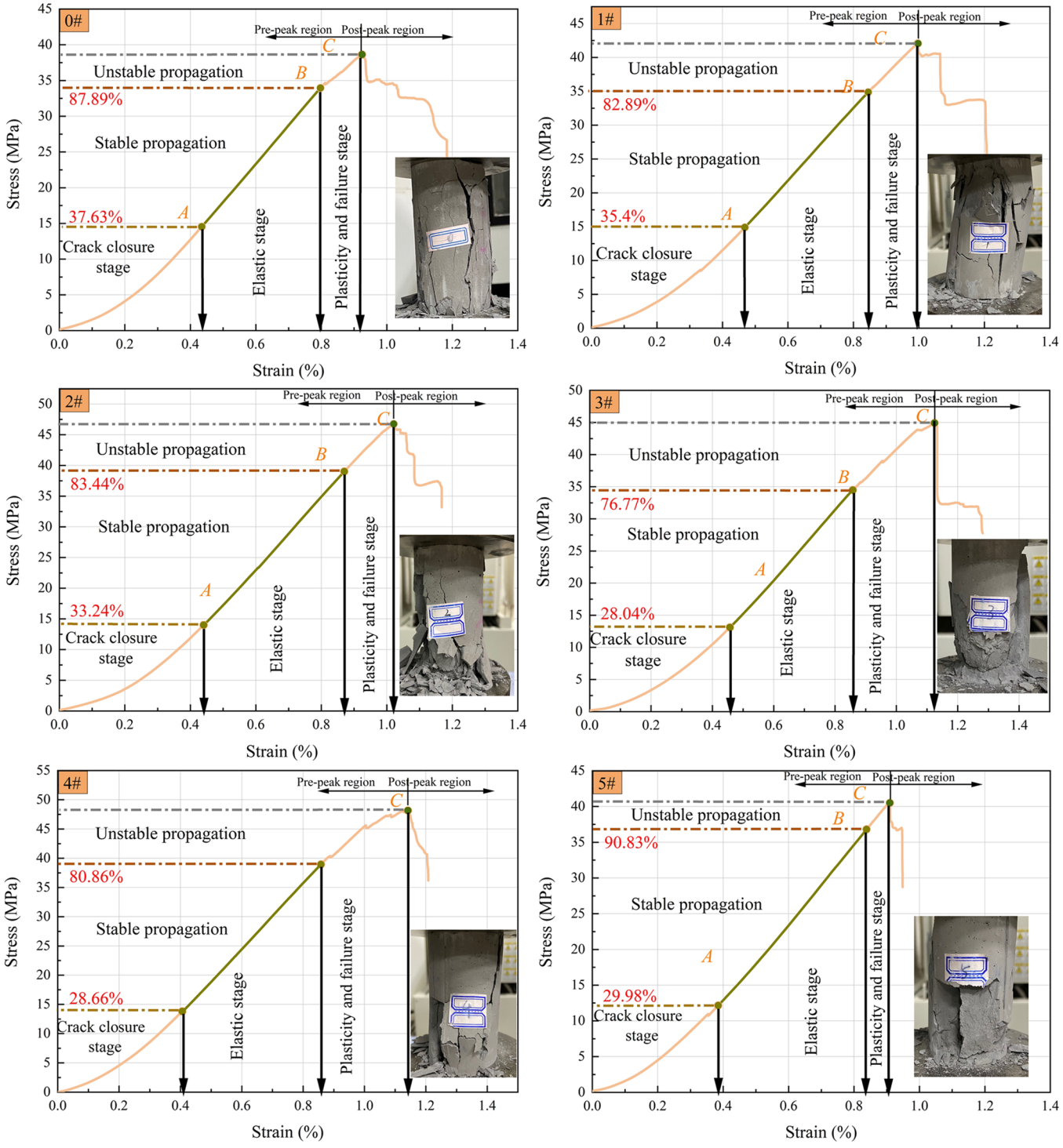

Figure 3. Stress−strain curves of drilling sealing materials with different nanomaterial ratios.

Table 3. Peak Stress of Sealing Materials under Different Curing Times

peak stress under different curing times (MPa)	#0	#1	#2	#3	#4	#5
7 d peak stress	25.58	28.68	33.09	31.02	33.82	27.74
28 d peak stress	38.62	42.07	46.75	44.92	48.16	40.51

elastic modulus and material compactness is shown in Figure 4. The elastic modulus of the material is negatively related to the porosity, and the value of the elastic modulus gradually decreases as the porosity increases. Therefore, the synergistic effect of nanomaterials improves the elastic modulus of materials, reduces the porosity of materials, and has a positive effect on the deformation resistance of materials.

3.2. X-ray Diffraction Analysis. Figure 5 shows the use of XRD to detect the main chemical and mineral components formed in cement under the synergistic effect of multiple nanomaterials. As shown in Figure 5, the main characteristic peaks include SiO_2, ettringite (AFt), calcium hydroxide (CH),

https://doi.org/10.1021/acsomega.2c01900
ACS Omega 2022, 7, 27991−28002

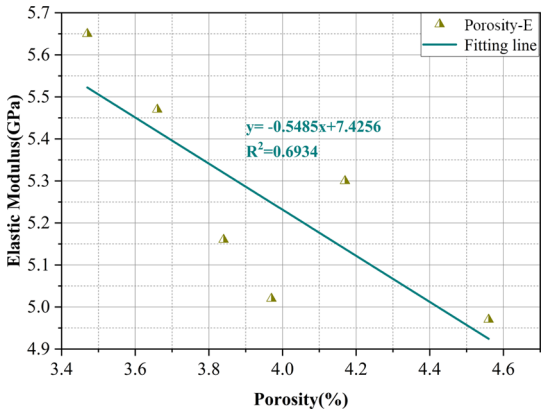

Figure 4. Relationship between the material porosity and elastic modulus.

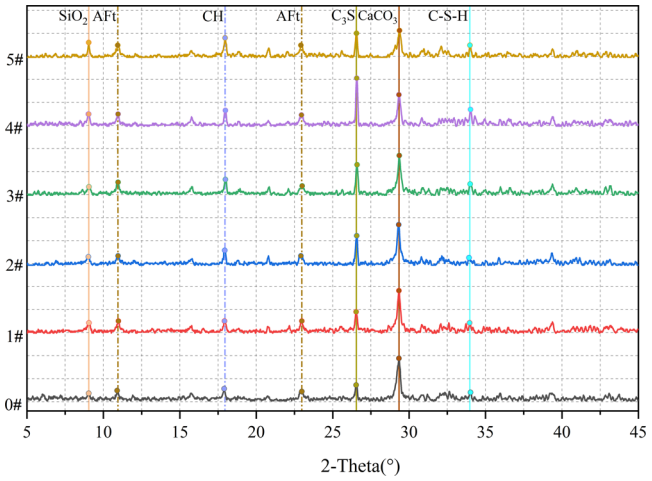

Figure 5. Comparison of XRD curves of drilling sealing materials with different nanomaterial ratios.

tricalcium silicate (C_3S), and $CaCO_3$ phases. These typical hydration products are consistent with other research results and do not produce new hydration products.[47,48]

Cement consumes a large amount of mineral components such as silicate and gypsum in the early stage of hydration and generates a large amount of hydrates such as C−S−H, CH, and AFt. The hydration products C−S−H and AFt in Portland cement can optimize the microscopic pore structure, while CH easily dissolves to form a porous structure and weakens the binding force between the C−S−H gel and concrete particles.[49,50] Due to the negative charge interaction between MWCNTs and OH^{-1}, the electrostatic repulsion between MWCNTs and superplasticizer molecules is affected, causing MWCNTs to agglomerate and reduce the strength of the modified material. Therefore, excessive CH in the modified material will have a greater negative impact on the strength. The addition of NS promotes the hydration reaction of cement, consumes calcium hydroxide, promotes the conversion of calcium silicate hydrate, and increases the C−S−H gel content at the interface between MWCNTs and the cement matrix.[51,52]

In the modified composite material, the intensity of the #4 CH peak reached the minimum, which indicates that the strongest pozzolanic reaction occurred in the sample, which consumed a large amount of CH to generate C−S−H gel. Due to the oxygen-containing functional groups on the surface of GO, CO_2 and H_2O will be released during the hydration reaction, and CO_2 will further consume CH in a large amount, reducing the negative impact of CH on the strength and increasing the compactness and mechanical properties of the material. As the content of C_3S increases, C_3S participates in the hydration reaction to generate more C−S−H gel and CH at room temperature. Then, more CH and SiO_2 participate in the reaction, and the subsequent participation in the hydration reaction will generate more C−S−H gel.[53,54] The order of diffraction peak $2\theta 1/4$ 22° of the tricalcium silicate (C_3S) peak of the cement mortar sample in Figure 5 is #4 > #2 > #3 > #5 > #1 > #0, compared with the $2\theta 1/434°$ diffraction peak characterizing the C−S−H gel content where this view is also confirmed. The synergistic effect of SiO_2 and GO nanomaterials has a better promotion effect on the formation of C−S−H gel.[55,56] Figure 5 shows that the #4 modified material with the ratio of 2 wt % SiO2, 0.1 wt % MWCNTs, and 0.03 wt % GO produced more hydration products such as C−S−H gels and Aft compared to the other samples. Therefore, the filling effect of the microscopic pore structure is the best, which is also consistent with the performance of the mechanical properties.

From the above analysis, NS and GO can be seen to promote the hydration reaction of cement under the condition of a synergistic effect in cement composite materials. C_3S, CH, gypsum, and other mineral components in cement are consumed to generate AFt, C−S−H gel, and other hydration products, which fill the microscopic pore structure and improve the compactness of the material. The hydration reaction mechanism is shown in Figure 6.

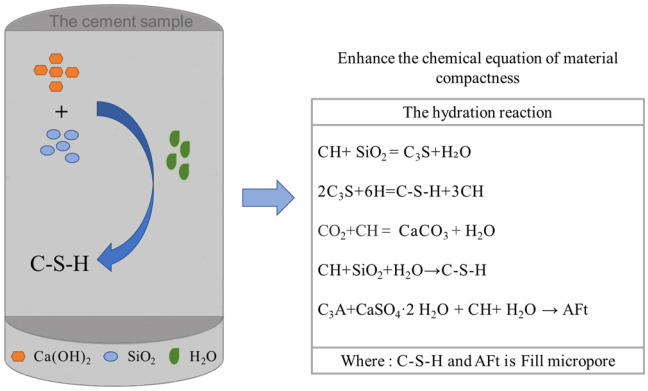

Figure 6. Mechanism of the hydration reaction of cement-based materials.

3.3. NMR Analysis and Discussion. *3.3.1. Material Porosity Characteristics.* The porosity of the six groups of specimens was measured through experiments. Table 4 shows

Table 4. Porosity of Sealing Materials in Different Proportion Schemes

sample	#0	#1	#2	#3	#4	#5
porosity (%)	4.56	3.84	4.17	3.97	3.47	3.66

the total porosity of each experimental group. The average porosity of the common cement material was 4.56%, and the total porosities of #1, #2, #3, #4, and #5 decreased by 15.8%, 8.5%, 12.9%, 23.9% and 19.7%, respectively, by adding different ratios of GO, SiO_2, and MWCNTs. Compared with the relatively single ratio of #1, #2, and #3, #4 and #5 have smaller porosities and the decrease in seepage pore volume is more

https://doi.org/10.1021/acsomega.2c01900
ACS Omega 2022, 7, 27991−28002

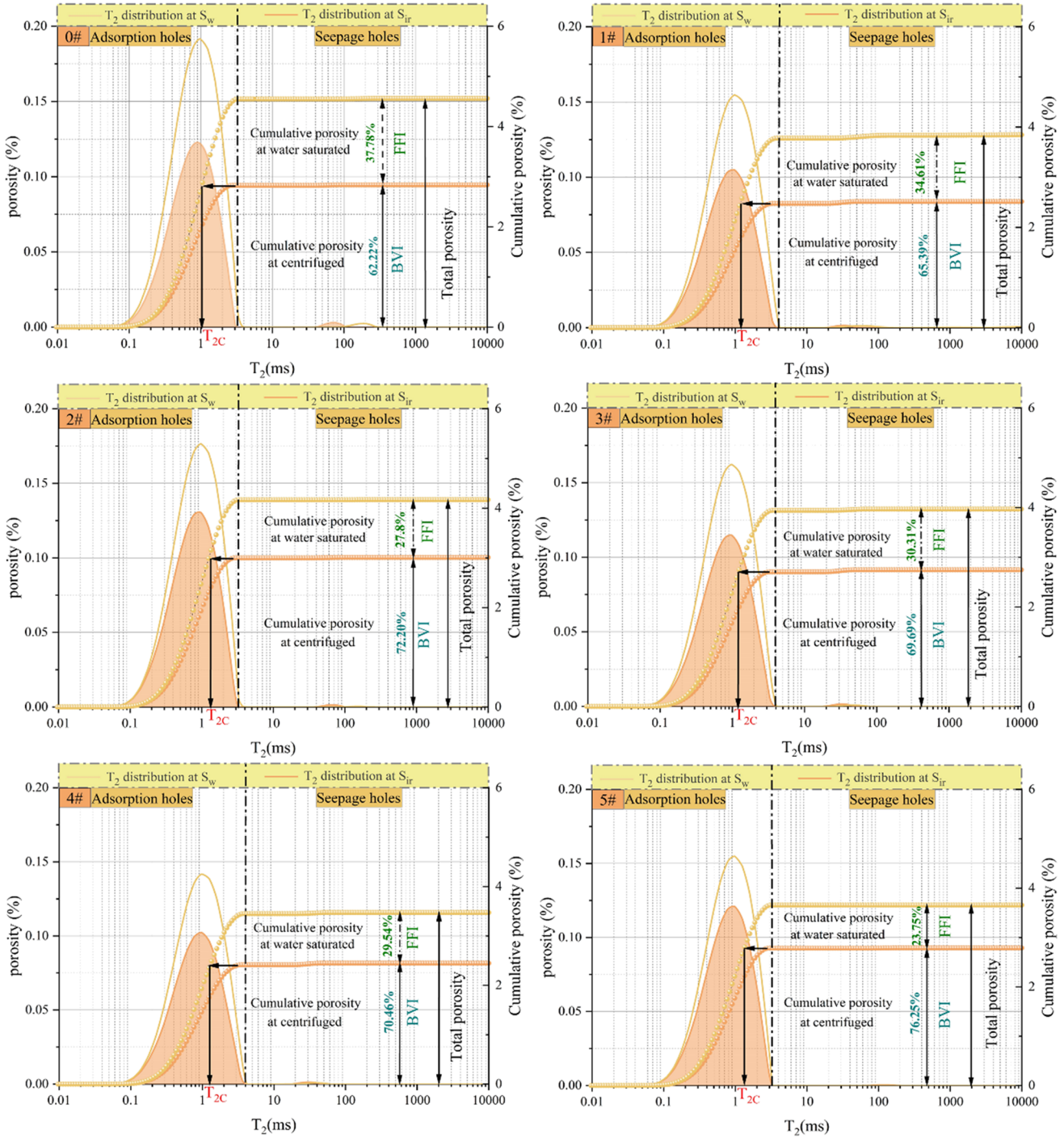

Figure 7. NMR curves under different nanomaterial ratios.

obviously reduced to 29.54% and 23.75%, respectively. The changes in these parameters show that the synergistic effect of the three nanomaterials can better optimize the pore structure of the sealing materials.

Figure 7 shows the porosity component and cumulative porosity curve where FFI and BVI represent the free fluid index (free water) and bound volume index (bound water), respectively, in pores.[57] Bound water corresponds to adsorption pores (capillary pores) that are not easy to drain; free water corresponds to seepage pores. In this paper, BVI is used to represent the ratio of the volume of adsorbed pores corresponding to the bound water in the specimen to the total pores, and FFI represents the ratio of the percolation pore volume corresponding to the free fluid to the total pore volume.

The T_2 cutoff value is a relaxation time threshold that divides the T_2 spectrum into two parts: bound water and free water. The size of this value is positively related to the number of adsorption holes and negatively correlated with the number of seepage pores. The method for determining the cutoff value of T_2 is shown in Figure 7. Due to the decrease in total porosity, the FFI value of the seepage pore volume decreases relatively, and the T_2 cutoff values of experimental groups #1, #2, #3, #4, and #5 are all shifted to the right in the coordinate axis compared with experimental group #0, indicating that the number of seepage

https://doi.org/10.1021/acsomega.2c01900
ACS Omega 2022, 7, 27991−28002

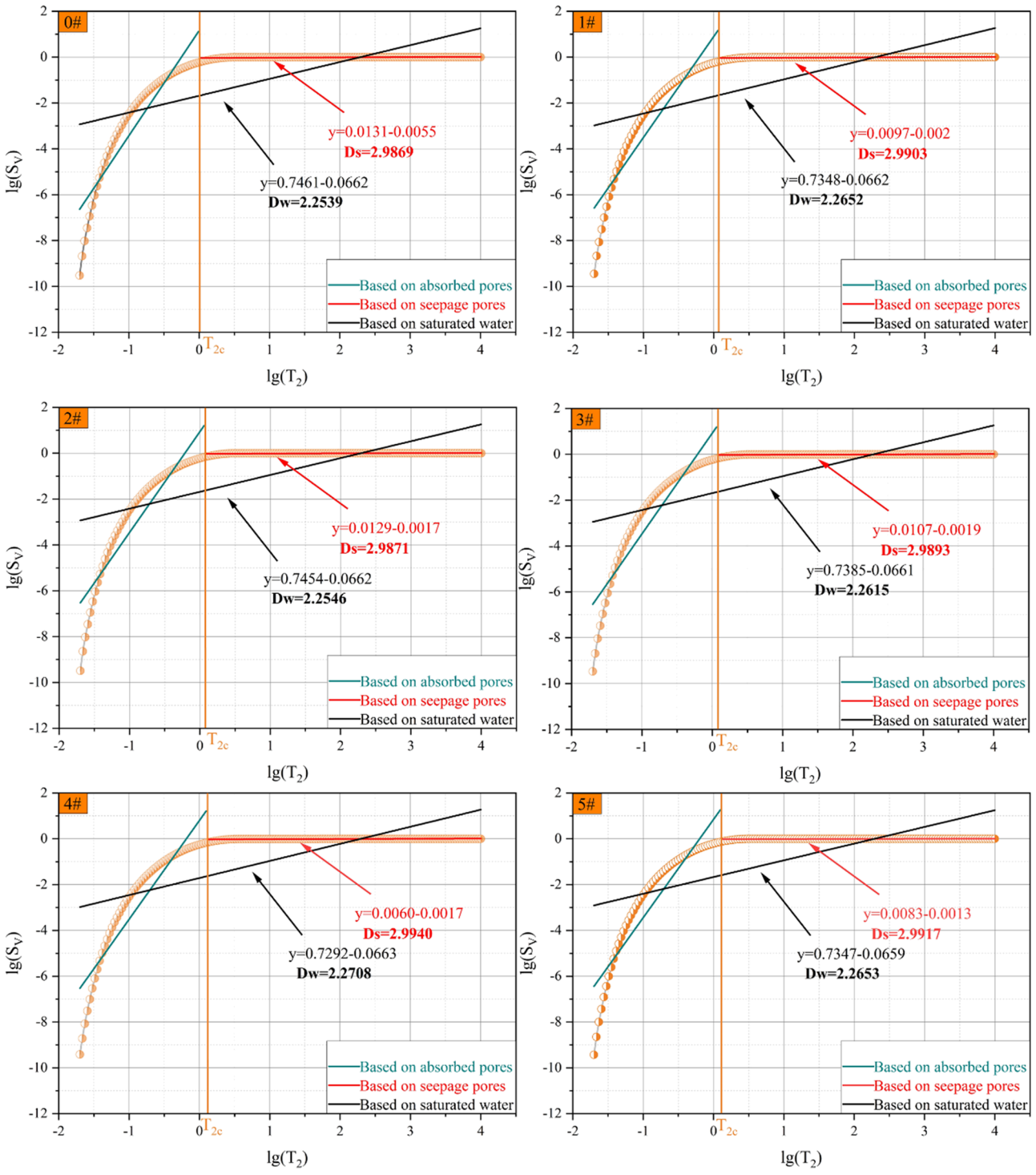

Figure 8. Pore fractal dimension curve based on NMR measurements.

holes is further reduced. The space volume ratio of the free fluid in the material is relatively reduced, and the space volume ratio of the bound fluid is relatively increased. Since the pore structure of the adsorption space is much more complicated than the pore structure of the seepage space, macroscopically, the pores of macropores and mesopores in the material can be considered to be closed or the pore volumes of macropores and mesopores are reduced, the difficulty of gas passing through the material is increased, and the compactness is further improved. That is, within a certain ratio range, the addition of three different nanomaterials is beneficial to reducing the generation of macropores and mesopores and improving the compactness of the material.

3.3.2. Characteristics of the Fractal Dimension of NMR. As shown in Figure 8, the cutoff time T_{2c} of T_2 represents the boundary between the bound fluid pores and the free fluid pores of the cement specimen. T_{2c} can divide the logarithmic relationship curve between S_v and T_2 into two parts, corresponding to adsorption pores and seepage pores. Based on the correlation between the adsorption pores and the seepage

https://doi.org/10.1021/acsomega.2c01900
ACS Omega 2022, 7, 27991−28002

pores, the fractal dimensions related to the adsorption pores and the seepage pores are calculated with T_{2c} as the boundary.[58,59] The fractal dimension of NMR of the cement sample is divided into D_w, based on the saturated water state, D_a, based on the bound water state, and D_s, based on the free water state, corresponding to the fractal dimension characteristics of total pores, adsorption pores, and seepage pores. The fractal dimension D_w (2.2539−2.2707) based on the saturated water state has an average value of 2.2623, and the fractal dimension D_s (2.9761−2.9917) based on the free water state has an average value of 2.9889, both of them conforming to the characteristics of the fractal dimension. The correlation coefficient of linear fitting of the fractal dimension of the seepage pores (0.8482−0.8630) is greater than the correlation coefficient of the total pores (0.4279−0.4406), so their fractal characteristics are more obvious. Because the D_a value based on the state of bound water is not in the range of 2−3, it will not be discussed in this article.

The size of the fractal dimension can reflect the complexity of the pore structure and the gas adsorption ability. The experimental data analysis shows that the fractal dimension of cement-based materials is negatively correlated with porosity. When the fractal dimension is in the range of 2−3, the closer it is to 2, the weaker the anisotropy, the more uniform the pore structure, and the better the connectivity between the pores. Conversely, the closer the fractal dimension is to 3, the more complex the pore structure of the specimen, the stronger the anisotropy, and the better the sealing.[60]

Table 5 shows the fractal dimension size of different cement-based sealing materials. The D_w and D_s values of the

Table 5. Fractal Dimension of Materials Based on NMR Spectra

	based on saturated water		based on seepage water	
sample	R^2	D_w	R^2	D_s
#0	0.4335	2.2539	0.8630	2.9869
#1	0.4406	2.2652	0.8596	2.9903
#2	0.4339	2.2546	0.8567	2.3987
#3	0.4330	2.2615	0.8569	2.9893
#4	0.4405	2.2708	0.8567	2.9940
#5	0.4279	2.2653	0.8482	2.9917

nanomodified materials #1, #2, #3, #4, and #5 all have different degrees of increase compared with the pure cement specimen #0. The reason for this phenomenon may be that nanoSiO_2 and GO have large specific surface areas with numerous hydrocarbon groups and unsaturated bonds and they can be adsorbed in the pores and promote the formation of hydration products in the pores. Furthermore, the generated C−S−H gel, AFt, and other hydrates are attached to the MWCNTs to form a network structure to inhibit the generation of cracks and pores, hinder the communication between pores, and increase the uneven and irregular pore morphology in the sample. The fractal dimensions D_w and D_s increase, which increases the difficulty of pore permeability. Therefore, within a certain proportion range, the content of nanomaterials in cement specimens is positively correlated with fractal dimensions D_w and D_s and negatively correlated with the porosity of cement samples.

Through orthogonal experimental comparison, the synergistic effect of adding graphene oxide, SiO_2, and MWCNT nanomaterials to the material is found to promote the generation of hydration products such as AFt and C−S−H gel and attachment to MWCNTs to form a network structure, which optimizes microscopic pores. With increasing D_w and D_s values, the material pores are more complicated, the difficulty of gas passing through the pores increases and the sealing performance is improved.

3.3.3. Relationship between Material Porosity, Peak Stress, and Fractal Dimension. As shown in Figure 9, the fractal

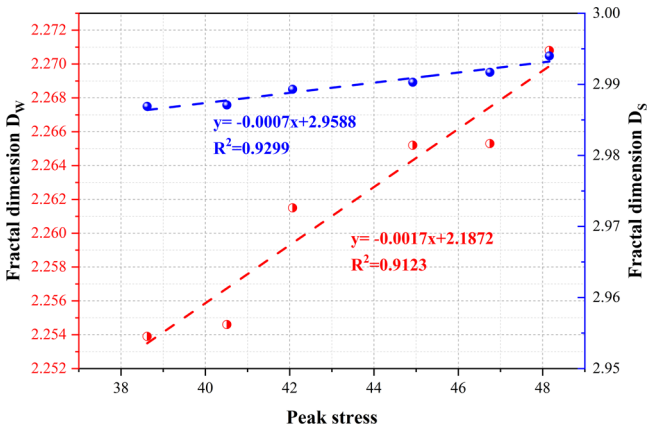

Figure 9. Relationship between the peak stress and fractal dimension.

dimension has a linear positive correlation with the peak stress. SiO_2, MWCNT, and GO nanomaterials enhance the connectivity between the internal aggregate of the sealing material and the binder, resulting in an increase in the fractal dimension. The synergistic effect of nanomaterials makes the hydration products and MWCNTs form a network structure to strengthen the mechanical strength of the material. Therefore, the peak stress and fractal dimension of the material increase accordingly.

Figure 10 shows the relationship between the porosity, elastic modulus, and fractal dimension. Both the porosity and elastic modulus are negatively correlated with the fractal dimension. With the increase of the fractal dimensions D_w and D_s, the total porosity and seepage porosity of the material decrease and the adsorption pores increase, making the distribution of pores more complicated, and the compactness of the sealing material itself is improved. As the pore complexity of the sealing material is increased, the connectivity is reduced, and the source of large pores and cracks generated by external force is reduced. Therefore, the ability of the sealing material to resist deformation is improved, and the elastic modulus value is also increased accordingly.

4. CONCLUSIONS

In this study, NSs, MWCNTs, and GO were mixed into cement composite materials in a certain proportion to modify the cement. Through uniaxial compression, XRD, NMR, and other technologies, the porosity of the material and the microscopic aspects of hydration products were combined with the macrophysical properties of the material for qualitative and quantitative analysis. The main conclusions are as follows.

(1) Compared with pure cement specimens, the total porosity of nanocement-based modified materials decreased to varying degrees, which played a positive role in improving the peak stress. Among these specimens, the total porosity of modified material #4 with the optimal ratio of 2 wt % NS, 0.1 wt % MWCNTs, and 0.03 wt % was reduced by 23.9%, the relative porosity was reduced by 8.16%, and the mechanical properties were improved by 24.7%.

https://doi.org/10.1021/acsomega.2c01900
ACS Omega 2022, 7, 27991−28002

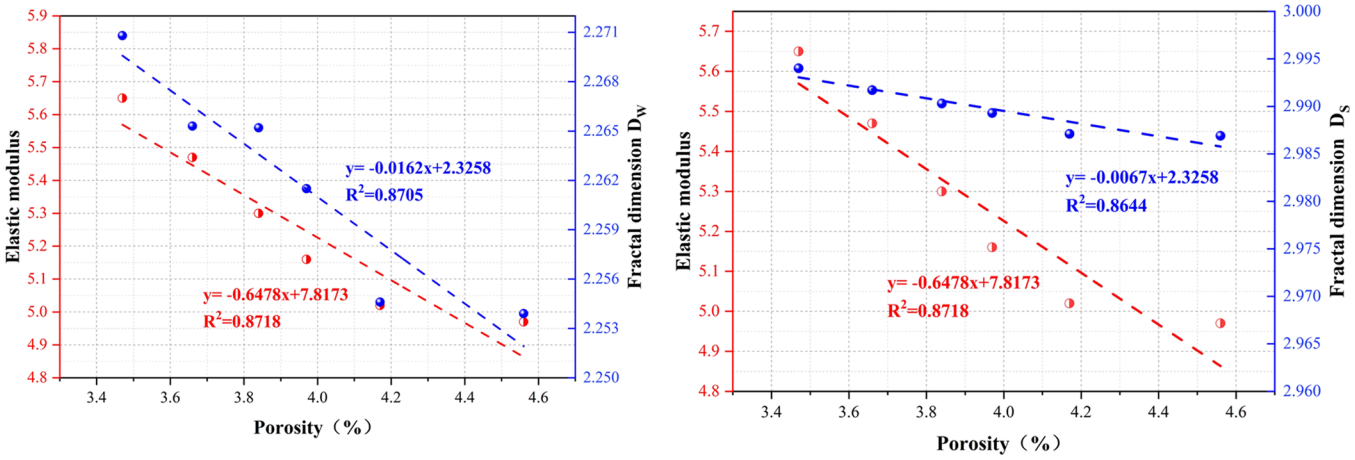

Figure 10. Relationship between the porosity, elastic modulus, and fractal dimension.

(2) When the mass percentage of SiO_2 in the nanocement-based composite modification materials increases from 2 to 4 wt %, the increased mass percentage will have a negative effect. The peak stress of the material under uniaxial compression decreases from 46.75 to 40.51 MPa with a decrease ratio of 13.35%, which may be due to the addition of excessive SiO_2 producing an agglomeration phenomenon, resulting in a decrease in the homogeneity of the specimen, thereby affecting the peak stress.

(3) As the addition of nanomaterials consumes a large amount of mineral components such as C_3S, CH, gypsum, etc., hydration products such as C−S−H gel and AFt are generated. The hydration products and MWCNTs together form a network structure to optimize microscopic pores and effectively inhibit the formation of macropores, mesopores, and cracks.

(4) The synergy of nanomaterials increases the total pore fractal dimension (D_w) and the seepage pore fractal dimension (D_s). The fractal dimension is negatively correlated with the porosity and positively correlated with the peak stress. Therefore, the synergistic effect of the three nanomaterials optimizes the pore structure of the sealing material and reduces the pore connectivity. The density and mechanical properties of the material are improved.

AUTHOR INFORMATION

Corresponding Author

Jun Xie − *College of Mining and Safety Engineering, Shandong University of Science and Technology, Qingdao 266590, China;* orcid.org/0000-0003-1864-0252; Email: xiejunsdust@sdust.edu.cn; Fax: +86 15898827668

Author

Dahe Yu − *Guizhou Ansheng Energy Co., Ltd., Guiyang, Guizhou 550000, China; Guizhou Jinsha Longfeng Coal Industry Co., Ltd., Jinsha, Guizhou 551800, China*

Complete contact information is available at: https://pubs.acs.org/10.1021/acsomega.2c01900

Notes

The authors declare no competing financial interest.

ACKNOWLEDGMENTS

This work is financially supported by the National Natural Science Foundation of China (nos. 52174192 and 51934004), the Shandong Provincial Natural Science Foundation (no. ZR2021YQ37), the National Key Research and Development Program of China (no. 2017YFC0805201), and the China Postdoctoral Science Foundation (nos. 2019T120599).

REFERENCES

(1) Bao, D.; Qiu, Z. S.; Zhao, X.; Zhong, H. Y.; Chen, J. X.; Liu, J. Y. Experimental investigation of sealing ability of lost circulation materials using the test apparatus with long fracture slot. *J. Petrol. Sci. Eng.* **2019**, *183*, 106396.

(2) Zhou, A. T.; Wang, K. A new inorganic sealing material used for gas extraction borehole. *Inorg. Chem. Commun.* **2019**, *102*, 75−82.

(3) Zhou, P. L.; Zhang, Y. H.; Huang, Z. A.; Gao, Y. K.; Wang, H.; Luo, Q. Coal and gas outburst prevention using new high water content cement slurry for injection into the coal seam. *Int. J. Min. Sci. Technol.* **2017**, *27*, 669−673.

(4) Zhao, Y.; Taheri, A.; Karakus, M.; Chen, Z. W.; Deng, A. Effects of water content, water type and temperature on the rheological behaviour of slag-cement and fly ash-cement paste backfill. *Int. J. Min. Sci. Technol.* **2020**, *30*, 271−278.

(5) Qin, B. T.; Lu, Y. Experimental research on inorganic solidified foam for sealing air leakage in coal mines. *Int. J. Min. Sci. Technol.* **2013**, *23*, 151−155.

(6) Tang, S. W.; Huang, J. S.; Duan, L.; Yu, P.; Chen, E. A review on fractal footprint of cement-based materials. *Powder Technol.* **2020**, *370*, 237−250.

(7) Li, G. X.; Liu, Q. F.; Niu, M. D.; Cao, L.; Nan, B.; Shi, C. Characteristic of silica nanoparticles on mechanical performance and microstructure of sulphoaluminate cement/ordinary Portland cement binary blends. *Constr. Build. Mater.* **2020**, *242*, 118158.

(8) Zhang, B. L.; Tan, H. B.; Shen, W. G.; Xu, G. L.; Ma, B. G.; Ji, X. L. Nano-silica and silica fume modified cement mortar used as Surface Protection Material to enhance the impermeability. *Cem. Concr. Compos.* **2018**, *92*, 7−17.

(9) Kooshafar, M.; Madani, H. An investigation on the influence of nano silica morphology on the characteristics of cement composites. *J. Build. Eng.* **2020**, *30*, 101293.

(10) Fernández, J. M.; Duran, A.; Navarro-Blasco, I.; Lanas, J.; Sirera, R.; Alvarez, J. I. Influence of nanosilica and a polycarboxylate ether superplasticizer on the performance of lime mortars. *Cem. Concr. Compos.* **2013**, *43*, 12−24.

(11) Arrechea, S.; Guerrero-Gutiérrez, E. M. A.; Velásquez, L.; Cardona, J.; Posadas, R.; Callejas, K.; Torres, S.; Díaz, R.; Barrientos, C.; García, E. Effect of additions of multiwall carbon nanotubes (MWCNT, MWCNT-COOH and MWCNT-Thiazol) in mechanical

compression properties of a cement-based material. *Materialia* **2020**, *11*, 107739.
(12) Jeevanagoudar, Y. V.; Krishna, R. H.; Gowda, R.; Preetham, R.; Prabhakara, R. Improved mechanical properties and piezoresistive sensitivity evaluation of MWCNTs reinforced cement mortars. *Constr. Build. Mater.* **2017**, *144*, 188−194.
(13) Shi, T.; Li, Z. X.; Guo, J.; Gong, H.; Gu, C. P. Research progress on CNTs/CNFs-modified cement-based composites − A review. *Constr. Build. Mater.* **2019**, *202*, 290−307.
(14) Long, W. J.; Wei, J. J.; Xing, F.; Khayat, K. H. Enhanced dynamic mechanical properties of cement paste modified with graphene oxide nanosheets and its reinforcing mechanism. *Cem. Concr. Compos.* **2018**, *93*, 127−139.
(15) Chen, Z. S.; Zhou, X.; Wang, X.; Guo, P. Mechanical behavior of multilayer GO carbon-fiber cement composites. *Constr. Build. Mater.* **2018**, *159*, 205−212.
(16) Zhai, C.; Yu, X.; Ni, G. H.; Li, M.; Hao, Z. Y. Microscopic properties and sealing performance of new gas drainage drilling sealing material. *Int. J. Min. Sci. Technol.* **2013**, *23*, 475−480.
(17) Ni, G. H.; Xie, H. C.; Li, S.; Sun, Q.; Huang, D. M.; Cheng, Y. Y.; Wang, N. The effect of anionic surfactant (SDS) on pore-fracture evolution of acidified coal and its significance for coalbed methane extraction. *Adv. Powder Technol.* **2019**, *30*, 940−951.
(18) Ni, G. H.; Dong, K.; Li, S.; Sun, Q.; Huang, D. M.; Wang, N.; Cheng, Y. Y. Development and performance testing of the new sealing material for gas drainage drilling in coal mine. *Powder Technol.* **2020**, *363*, 152−160.
(19) Zhai, C.; Hao, Z. Y.; Lin, B. Q. Research on a New Composite Sealing Material of Gas Drainage Borehole and Its Sealing Performance. *Procedia Eng.* **2011**, *26*, 1406−1416.
(20) Li, Z.; Ni, G. H.; Sun, L. L.; Sun, Q.; Li, S.; Dong, K.; Xie, J. N.; Wang, G. Effect of ionic liquid treatment on pore structure and fractal characteristics of low rank coal. *Fuel* **2020**, *262*, 116513.
(21) Jiang, H. H.; Ni, G. H.; Zhu, C. J.; Zhang, X. F.; Sun, G. S.; Wang, Z. Y.; Huang, Q. M. Molecular dynamics simulations and experimental characterization of the effect of different concentrations of [Bmim][Cl] in aqueous solutions on the wettability of anthracite. *Fuel* **2022**, *324*, 124618.
(22) Aodkeng, S.; Sinthupinyo, S.; Chamnankid, B.; Hanpongpun, W.; Chaipanich, A. Effect of carbon nanotubes/clay hybrid composite on mechanical properties, hydration heat and thermal analysis of cement-based materials. *Constr. Build. Mater.* **2022**, *320*, 126212.
(23) Ghirian, A.; Fall, M. Strength evolution and deformation behaviour of cemented paste backfill at early ages: Effect of curing stress, filling strategy and drainage. *Int. J. Min. Sci. Technol.* **2016**, *26*, 809−817.
(24) Duan, H. F.; Jiang, Z. Q.; Zhu, S. Y.; Yao, P.; Sun, Q. New composite grouting materials: Modified urea−formaldehyde resin with cement. *Int. J. Min. Sci. Technol.* **2012**, *22*, 195−200.
(25) Cheng, W. M.; Sun, L. L.; Wang, G.; Du, W. Z.; Qu, H. Y. Experimental research on coal seam similar material proportion and its application. *Int. J. Min. Sci. Technol.* **2016**, *26*, 913−918.
(26) Chen, X.; Shi, X. Z.; Zhou, J.; Li, E. M.; Qiu, P. Q.; Gou, Y. G. High strain rate compressive strength behavior of cemented paste backfill using split Hopkinson pressure bar. *Int. J. Min. Sci. Technol.* **2021**, *31*, 387−399.
(27) Liu, X. Y.; Liu, L.; Lyu, K.; Li, T. Y.; Zhao, P. Z.; Liu, R. D.; Zuo, J. Q.; Fu, F.; Shah, S. P. Enhanced early hydration and mechanical properties of cement-based materials with recycled concrete powder modified by nano-silica. *J. Build. Eng.* **2022**, *50*, 104175.
(28) Xiang, X. W.; Zhai, C.; Xu, Y. M.; Yu, X.; Xu, J. Z. A flexible gel sealing material and a novel active sealing method for coal-bed methane drainage boreholes. *J. Nat. Gas. Sci. Eng.* **2015**, *26*, 1187−1199.
(29) Dong, K.; Ni, G. H.; Xu, Y. H.; Xun, M.; Wang, H.; Li, S.; Sun, Q.; Li, Y. F. Effect of nano-SiO_2/styrene-acrylic emulsion on compactness and strength of mine drilling seal materials. *Powder Technol.* **2020**, *372*, 325−335.
(30) Abhilash, P. P.; Nayak, D. K.; Sangoju, B.; Kumar, R.; Kumar, V. Effect of nano-silica in concrete; a review. *Constr. Build. Mater.* **2021**, *278*, 122347.
(31) Naqi, A.; Abbas, N.; Zahra, N.; Hussain, A.; Shabbir, S. Q. Effect of multi-walled carbon nanotubes (MWCNTs) on the strength development of cementitious materials. *J. Mater. Res. Technol.* **2019**, *8*, 1203−1211.
(32) Zhao, L.; Guo, X. L.; Song, L. G.; Song, Y.; Dai, G. Z.; Liu, J. P. An intensive review on the role of graphene oxide in cement-based materials. *Constr. Build. Mater.* **2020**, *241*, 117939.
(33) Ni, G. H.; Li, S.; Rahman, S.; Xun, M.; Wang, H.; Xu, Y. H.; Xie, H. C. Effect of nitric acid on the pore structure and fractal characteristics of coal based on the low-temperature nitrogen adsorption method. *Powder Technol.* **2020**, *367*, 506−516.
(34) Li, Z.; Ni, G. H.; Wang, H.; Sun, Q.; Wang, G.; Jiang, B. Y.; Zhang, C. Molecular structure characterization of lignite treated with ionic liquid via FTIR and XRD spectroscopy. *Fuel* **2020**, *272*, 117705.
(35) Saleh, F. K.; Teodoriu, C.; Sondergeld, C. H. Investigation of the effect of cement mixing energy on cement strength and porosity using NMR and UPV methods. *J. Nat. Gas Sci. Eng.* **2019**, *70*, 102972.
(36) Yao, Y. B.; Liu, D. M. Comparison of low-field NMR and mercury intrusion porosimetry in characterizing pore size distributions of coals. *Fuel* **2012**, *95*, 152−158.
(37) Li, X. Z.; Lin, B. Q.; Zhai, C.; Ni, G. H.; Li, Z. W. Relaxation study of cement based grouting material using nuclear magnetic resonance. *Int. J. Min. Sci. Technol.* **2012**, *22*, 821−824.
(38) Ni, G. H.; Sun, Q.; Xun, M.; Wang, H.; Xu, Y. H.; Cheng, W. M.; Wang, G. Effect of NaCl-SDS compound solution on the wettability and functional groups of coal. *Fuel* **2019**, *257*, 116077.
(39) Ni, G. H.; Li, Z.; Sun, Q.; Li, S.; Dong, K. Effects of [Bmim][Cl] ionic liquid with different concentrations on the functional groups and wettability of coal. *Adv. Powder Technol.* **2019**, *30*, 610−624.
(40) Wang, X. Y.; Dong, S. F.; Ashour, A.; Zhang, W.; Han, B. G. Effect and mechanisms of nanomaterials on interface between aggregates and cement mortars. *Constr. Build. Mater.* **2020**, *240*, 117942.
(41) Zhao, L.; Guo, X. L.; Ge, C.; Li, Q.; Guo, L. P.; Shu, X.; Liu, J. P. Investigation of the effectiveness of PC@GO on the reinforcement for cement composites. *Constr. Build. Mater.* **2016**, *113*, 470−478.
(42) Lv, S. H.; Liu, J. J.; Sun, T.; Ma, Y. J.; Zhou, Q. F. Effect of GO nanosheets on shapes of cement hydration crystals and their formation process. *Constr. Build. Mater.* **2014**, *64*, 231−239.
(43) Han, W. B.; Zhou, G.; Zhang, Q. T.; Pan, H. W.; Liu, D. Experimental study on modification of physicochemical characteristics of acidified coal by surfactants and ionic liquids. *Fuel* **2020**, *266*, 116966.
(44) Xie, H. C.; Ni, G. H.; Xie, J. N.; Cheng, W. M.; Xun, M.; Xu, Y. H.; Wang, H.; Wang, G. The effect of SDS synergistic composite acidification on the chemical structure and wetting characteristics of coal. *Powder Technol.* **2020**, *367*, 253−265.
(45) Ghafari, E.; Costa, H.; Júlio, E.; Portugal, A.; Durães, L. The effect of nanosilica addition on flowability, strength and transport properties of ultra high performance concrete. *Mater. Des.* **2014**, *59*, 1−9.
(46) Liu, Z. X.; Dang, W. G.; Liu, Q. L.; Chen, G. H.; Peng, K. Optimization of clay material mixture ratio and filling process in gypsum mine goaf. *Int. J. Min. Sci. Technol.* **2013**, *23*, 337−342.
(47) Wang, B. M.; Deng, S. Effect and mechanism of graphene nanoplatelets on hydration reaction, mechanical properties and microstructure of cement composites. *Constr. Build. Mater.* **2019**, *228*, 116720.
(48) Chintalapudi, K.; Pannem, R. M. R. The effects of Graphene Oxide addition on hydration process, crystal shapes, and micro-structural transformation of Ordinary Portland Cement. *J. Build. Eng.* **2020**, *32*, 101551.
(49) Esteves, L. P. On the hydration of water-entrained cement−silica systems: Combined SEM, XRD and thermal analysis in cement pastes. *Thermochim. Acta* **2011**, *518*, 27−35.

https://doi.org/10.1021/acsomega.2c01900
ACS Omega 2022, 7, 27991−28002

(50) Li, S. J.; Zhang, Y. L.; Lin, S. S.; Yan, J.; Du, S. G. Effects of nano-SiO_2 coated multi-walled carbon nanotubes on mechanical properties of cement-based composites. *Constr. Build. Mater.* **2021**, *281*, 122577.
(51) Mendoza, O.; Sierra, G.; Tobón, J. I. Influence of super plasticizer and $Ca(OH)_2$ on the stability of functionalized multi-walled carbon nanotubes dispersions for cement composites applications. *Constr. Build. Mater.* **2013**, *47*, 771−778.
(52) Wang, J. B.; Liu, M. L.; Wang, Y. G.; Zhou, Z. H.; Xu, D. Y.; Du, P.; Cheng, X. Synergistic effects of nano-silica and fly ash on properties of cement-based composites[J]. *Constr. Build. Mater.* **2020**, *262*, 120737.
(53) Wang, X. L.; Gong, C. C.; Lei, J. G.; Dai, J.; Lu, L. C.; Cheng, X. Effect of silica fume and nano-silica on hydration behavior and mechanism of high sulfate resistance Portland cement. *Constr. Build. Mater.* **2021**, *279*, 122481.
(54) Xie, H.C.; Ni, G.H.; Li, S.; Sun, Q.; Dong, K.; Xie, J. N.; Wang, G.; Liu, Y.X. The influence of surfactant on pore fractal characteristics of composite acidized coal. *Fuel* **2019**, *253*, 741−753.
(55) Hu, S. Y.; Han, D. D.; Feng, G. R.; Zhang, A.; Hao, G. C.; Hu, L. Q.; Zhu, L. P.; Li, B. Influence of Stress on Void Ratios of Compacted Crushed Rock Masses in Coal Mine Gobs. *Nat. Resour. Res.* **2019**, *29*, 1361−1373.
(56) Xie, J. N.; Ni, G. H.; Xie, H. C.; Li, S.; Sun, Q.; Dong, K. The effect of adding surfactant to the treating acid on the chemical properties of an acid-treated coal. *Powder Technol.* **2019**, *356*, 263−272.
(57) Hughes, C. E.; Walkley, B.; Gardner, L. J.; Walling, S. A.; Bernal, S. A.; Iuga, D.; Provis, J. L.; Harris, K. D. M. Exploiting in-situ solid-state NMR spectroscopy to probe the early stages of hydration of calcium aluminate cement. *Solid. State. Nucl. Magn. Res.* **2019**, *99*, 1−6.
(58) Nie, B. S.; Lun, J. Y.; Wang, K. D.; Shen, J. S. Three-dimensional characterization of open and closed coal nanopores based on a multi-scale analysis including CO_2 adsorption, mercury intrusion, low-temperature nitrogen adsorption, and small-angle X-ray scattering. *Energy Sci. Eng.* **2020**, *8*, 2086−2099.
(59) Nie, B. S.; Ma, Y. K.; Hu, S. T.; Meng, J. Q. Laboratory Study Phenomenon of Coal and Gas Outburst Based on a Mid-scale Simulation System. *Sci. Rep.* **2019**, *9*, 15005.
(60) Gao, Y.; Jiang, J. Y.; De Schutter, G.; Ye, G.; Sun, W. Fractal and multifractal analysis on pore structure in cement paste. *Constr. Build. Mater.* **2014**, *69*, 253−261.

https://doi.org/10.1021/acsomega.2c01900
ACS Omega 2022, 7, 27991−28002